# Cation distribution in some natural spinels from X-ray diffraction and Mössbauer spectroscopy

SUSANNA CARBONIN

Dipartimento di Mineralogia e Petrologia, Università di Padova, Corso Garibaldi 37, 35122 Padua, Italy

UMBERTO RUSSO

Dipartimento di Chimica Inorganica, Metallorganica e Analitica, Università di Padova, Via Loredan 4, 35131 Padua, Italy

AND

ANTONIO DELLA GIUSTA

Dipartimento di Mineralogia e Petrologia, Università di Padova, Corso Garibaldi 37, 35122 Padua, Italy

## Abstract

Three natural spinels of different places of occurrence and compositions were investigated by means of microprobe chemical analysis, single crystal X-ray diffraction and Mössbauer spectroscopy. All cation distributions between *T* and *M* sites were calculated from microprobe and XRD experimental data, by means of a mathematical model with appropriate assumptions. $Fe^{2+}$ and $Fe^{3+}$ assignments calculated in this way were compared with those observed in Mössbauer spectra. The satisfactory agreement found proves, at least in the samples studied, the reliability of the model and the assumptions used. In the spinels examined, such results show $Fe^{2+}$ and $Fe^{3+}$ virtually ordered in *T* and *M* sites respectively. Mössbauer data also revealed $Fe^{2+}$ in different tetrahedral sites due to the next-nearest neighbour effect, probably as a consequence of spinel genetic conditions.

KEYWORDS: spinel, cation distribution, Mössbauer spectroscopy, X-ray diffraction.

## Introduction

CATION distribution in synthetic spinels has been investigated by several techniques:
the use of conductivity in tandem with Seebeck effect in ferrospinel solid solutions enabled complete characterization of up to four cations distributed between *T* and *M* sites (Mason, 1987; Nell *et al.*, 1989);
$^{27}Al$ and $^{17}O$ magic-angle spinning NMR allowed study of the temperature-dependent disorder of $MgAl_2O_4$ up to 1400°C (Millard *et al.*, 1992);
Mössbauer spectroscopy has been applied to determine $Fe^{2+}$ and $Fe^{3+}$ distribution and the $Fe^{3+}/Fe_{tot.}$ ratio (Bancroft *et al.*, 1983);
powder X-ray or neutron diffraction structural refinement, alone or associated with Mössbauer spectroscopy again, has been used by several authors to determine cation distribution (e.g. O'Neill *et al.*, 1991; Roelofsen *et al.*, 1992; Peterson *et al.*, 1991; O'Neill *et al.*, 1992; Waerenborgh *et al.*, 1994).

Comparatively little attention has been given to natural spinels, in spite of the useful information potentially supplied by their temperature-dependent intracrystalline distribution (O'Neill and Navrotsky, 1984; Ottonello, 1986). This is mainly because of difficulties in assigning major cations (e.g. Mg, Al, $Fe^{2+}$, $Fe^{3+}$) present to both tetrahedral and octahedral sites of the lattice. A further problem with natural spinels is the accurate determination of $Fe^{3+}$, which is crucial, at least in very sensitive cases (e.g. oxygen fugacity calculation; Wood and Virgo, 1989). Cation distribution determination therefore requires the combination of several complementary methods, as already done for orthopyroxenes (Skogby *et al.*, 1992).

*Mineralogical Magazine, April 1996, Vol. 60, pp. 355–368*

In this work, electron microprobe analysis, single crystal X-ray diffraction and Mössbauer spectroscopy were all used to obtain information on cation distribution in three natural spinels.

## Samples

The analysed spinels represent common compositions found in a large variety of rocks. Sample VASA is a greyish light-blue spinel from Kalkbro, Sweden (now in the Collezione del Museo di Mineralogia, Università di Padua). In the Kalkbro limestone it reaches 0.5 cm in size and is associated with abundant yellowish mica, chondrodite, pale amphibole, and rare pyroxene and anorthite (Lindqvist, personal communication). CR5 is a chromite from the Rustemberg mine, Cape Kamari, Bushveld Complex (Toffanin, 1989). TS2 comes from a suite of websteritic dykes crossing a peridotite of mainly lherzolitic composition in the Ivrea-Verbano area, Italian Western Alps (Pizzolon, 1991). This suite, named 'Al-augite suite' (Comin-Chiaramonti *et al.*, 1982) contains spinel with low Cr content, Cr/(Cr + Al) generally being < 0.04. Very slow cooling during uplift allowed strong exsolution phenomena to take place in the associated pyroxene, so that a highly ordered distribution is to be expected in these spinels.

## Electron microprobe analysis

All spinel analyses were obtained on the Cameca/Camebax electron microprobe at the Dept. of Mineralogy and Petrology of the University of Padua, at 15 kV and 15 nA beam current, using WDS spectrometers. Synthetic oxide standards were used, and results were monitored against the standards themselves. Analyses were carried out after a check to guarantee that $I_{Xstd}/I_{std} = 1.00 \pm 0.01$ for each element, where $I_{Xstd}$ is the intensity of the analysed standard and $I_{std}$ is the intensity of the same standard monitored after each element calibration. X-ray counts were converted into oxide weight percentages using the PAP correction program provided by Cameca. Analyses for major elements were typically accurate within 1% of the amount present and within 5% for minor elements. Results are reported in Table 1.

In order to gain understanding of sample homogeneity, analyses were performed on as many spinel crystals as possible.

From the VASA sample 13 crystals were extracted, from which a total of 67 spots were analysed. The sample showed good homogeneity, both within single grains and between grains. Composition was close to the spinel end-member, with $Fe^{2+}$–Mg as the only appreciable substitution. On the basis of stoichiometry, the amount of $Fe^{3+}$ calculated from the average of 67 analyses (0.008 a.f.u.) was virtually zero, being about equal to its standard deviation. The $Fe^{3+}/Fe_{tot.}$ ratio, (reported in Table 1 only for the sake of uniformity) has equally little value.

Five to ten analyses were performed on each of the twelve grains of chromite CR5, yielding a total of 71 points analysed. Homogeneity was less than that shown by VASA, mainly as far as Cr and Fe contents were concerned. In sample TS2 nearly 100 randomly chosen points were analysed on one thin section, without any bias as regards colour or size. Single grains were quite homogeneous, while the overall average composition showed quite high standard deviations for $Cr_2O_3$ and $Al_2O_3$ contents, even in the small area investigated ($\sim 2$ cm$^2$). Also the $Fe^{3+}/Fe_{tot.}$ ratio, calculated from stoichiometry, ranged extensively from one point to another.

## Single crystal X-ray diffraction

### *Experimental*

Several crystals were examined for single-crystal structural refinement. Dozens of crystals from sample TS2 had to be examined to find some suitable for single-crystal data collection. Since they presented relatively larger cell parameter variations, three of them (TS2A1, TS2E1, TS2F1) were chosen as representative of these variations. As shown below, all of them have Cr content lower than that reported in Table 1, obtained from a different chip of the same hand specimen. Only one crystal was investigated in each of the other two samples (VASA1, CR5A1).

Unit cell parameters were obtained with one of the standard programs of the single-crystal STOE AED4 diffractometer with monochromatized Mo-$K\alpha$ radiation. Twenty-two reflections in the range $8° < \theta < 20°$ were accurately centred, a step-scan through each reflection was made at positive $2\theta$ and $\omega$, and the centre of gravity was calculated. The reflection was then scanned at negative $2\theta$ and $\omega$, and again the centre was determined. The mean of the $\omega$ centres was taken as the true $\theta$ value. Continual calibrations were performed by means of a quartz crystal and a ruby supplied by the Organizing Committee of the XII Congress of the IUC. Diffraction data were collected on a STOE AED4 diffractometer up to $2\theta \cong 100°$. The $\omega$–$2\theta$ scan mode was used with peak-base widths of $2\theta = 2°$, 45-step integration, 0.6 s per step counting time. Six equivalent reflections were measured and corrected for absorption and background, following North *et al.* (1968) and Blessing *et al.* (1972) respectively. After correction for Lorentz and polarization effects and isotropic secondary extinction, a set of more than 170 observed structural

TABLE 1. Microprobe data of spinels (bulk compositions) and formulae on the basis of 3 cations and 4 oxygens

| | VASA | | CR5 | | TS2 | |
|---|---|---|---|---|---|---|
| | avg. 67 pts. | St.Dev. | avg. 71 pts. | St.Dev. | avg. 102 pts. | St.Dev. |
| $Al_2O_3$ | 69.97 | 0.25 | 14.40 | 0.20 | 62.43 | 1.31 |
| FeO | 4.05 | 0.15 | 25.89 | 0.40 | 14.96 | 0.79 |
| MgO | 25.52 | 0.25 | 9.87 | 0.21 | 19.81 | 0.57 |
| MnO | 0.11 | 0.04 | 0.27 | 0.09 | 0.05 | 0.04 |
| $SiO_2$ | 0.04 | 0.02 | 0.04 | 0.02 | 0.10 | 0.04 |
| ZnO | 0.36 | 0.09 | 0.10 | 0.07 | n.a. | n.a. |
| $Cr_2O_3$ | 0.02 | 0.02 | 48.50 | 0.48 | 2.48 | 1.12 |
| NiO | 0.02 | 0.03 | 0.11 | 0.05 | 0.34 | 0.06 |
| $TiO_2$ | 0.01 | 0.01 | 0.61 | 0.09 | 0.03 | 0.03 |
| Total | 100.09 | | 99.79 | | 100.20 | |
| Al | 1.990 | 0.007 | 0.550 | 0.007 | 1.870 | 0.026 |
| $Fe^{2+}$ | 0.074 | 0.006 | 0.527 | 0.010 | 0.244 | 0.016 |
| $Fe^{3+}$ | 0.008 | 0.007 | 0.175 | 0.009 | 0.074 | 0.009 |
| Mg | 0.918 | 0.007 | 0.477 | 0.009 | 0.751 | 0.016 |
| Mn | 0.002 | 0.001 | 0.007 | 0.002 | 0.001 | 0.001 |
| Si | 0.001 | 0.000 | 0.001 | 0.001 | 0.002 | 0.001 |
| Zn | 0.006 | 0.002 | 0.002 | 0.002 | n.a. | n.a. |
| Cr | 0.000 | 0.000 | 1.243 | 0.012 | 0.050 | 0.023 |
| Ni | 0.000 | 0.001 | 0.003 | 0.001 | 0.007 | 0.001 |
| Ti | 0.000 | 0.000 | 0.015 | 0.002 | 0.001 | 0.001 |
| Total | 3.000 | | 3.000 | | 3.000 | |
| $Fe^{3+}/Fe_{tot}$.avg. | 0.092 | 0.079 | 0.249 | 0.011 | 0.232 | 0.026 |
| $Fe^{3+}/Fe_{tot}$.min. | 0.000 | | 0.217 | | 0.164 | |
| $Fe^{3+}/Fe_{tot}$.Max. | 0.281 | | 0.272 | | 0.293 | |

Ratios in bottom rows calculated directly from microprobe data, with more decimal figures than shown above.

factors $Fo_{hkl}$ was obtained from each crystal (Table 2).

### *Crystal structure refinement*

Structural refinements were performed in the *Fd3m* space group, since no evidence of different symmetry appeared. The refined parameters were: scale factor, secondary extinction coefficient (*Ext. coeff.*), oxygen coordinate *u*, tetrahedral and octahedral site occupancies, displacement parameters *U*. Two scattering curves, Mg *vs.* Fe in the *T* site and Al *vs.* Cr or Fe (for CR5 and TS2, respectively) in the *M* site, were assigned to sites involved in isomorphous replacements, with the constraint of full site occupancy and equal displacement parameters. No constraint from chemical analyses was imposed.

Calculations executed against $Fo_{hkl}$ turned out to be rather unstable, and dependent on the $\sigma$ threshold used. Consequently, structural refinements were performed against $Fo^2_{hkl}$ using the SHELX-93 program (Sheldrick, 1993). Recovering all information from the relatively large number of weak reflections, stable refinements were obtained and all correlations involving site occupancies disappeared, allowing simultaneous minimization of all structural parameters. Site occupancies only depended slightly on the ionization level of the oxygen scattering curve, while the cation ionization level was irrelevant except in sample CR5A1, in which it showed a slight influence.

Refinements of all crystals were repeated systematically, changing the scattering curves to obtain the best values of all conventional agreement factors over all $\sin\theta/\lambda$ intervals.

The best results were obtained with neutral cations and $O^{-1.4}$ in samples VASA1 and TS2, although CR5A1, with large amounts of Fe and Cr, required fully ionized cations and $O^{-1.6}$. The best result in VASA1 was obtained by assigning only Al to the *M* site and by changing its occupancy factor.

TABLE 2. Crystallographic data of spinels

| | VASA1 | CR5A1 | TS2A1 | TS2E1 | TS2F1 |
|---|---|---|---|---|---|
| $a$ (Å) | 8.0930(3) | 8.3017(5) | 8.1104(5) | 8.1081(5) | 8.1122(4) |
| $u$* | 0.26353(6) | 0.26274(12) | 0.26362(7) | 0.26363(5) | 0.26359(6) |
| 2θ max.(°) | 106 | 100 | 104 | 105 | 105 |
| $R_{4\sigma}$ | 0.0288 | 0.0305 | 0.0301 | 0.0203 | 0.0292 |
| $R_{all}$ | 0.0326 | 0.0346 | 0.0318 | 0.0230 | 0.0300 |
| $N_{4\sigma}(N_{all})$ | 169(184) | 153(174) | 172(180) | 168(181) | 173(182) |
| *Ext. coeff.* | 0.01994 | 0.02991 | 0.00916 | 0.00403 | 0.01188 |
| $U_{11}(Ox)$ | 0.00694(14) | 0.00964(31) | 0.00865(16) | 0.00754(12) | 0.00915(15) |
| $U_{12}(Ox)$ | −0.00016(10) | −0.00082(22) | −0.00035(12) | −0.00033(10) | −0.00024(11) |
| $U_{eq}(Ox)$ | 0.00694(14) | 0.00964(31) | 0.00865(16) | 0.00754(12) | 0.00915(15) |
| $U_{11}$(M) | 0.00607(13) | 0.00775(16) | 0.00735(16) | 0.00622(13) | 0.00757(16) |
| $U_{12}$(M) | −0.00040(7) | −0.00038(7) | −0.00034(8) | −0.00026(6) | −0.00041(7) |
| $U_{eq}$(M) | 0.00607(13) | 0.00775(16) | 0.00735(16) | 0.00622(13) | 0.00757(16) |
| $U_{11}$(T) | 0.00714(22) | 0.01006(27) | 0.00858(21) | 0.00763(16) | 0.00883(20) |
| Occ.(M) | 0.998(4) | 0.268(18) | 0.971(4) | 0.972(3) | 0.966(4) |
| $e$(M) | 12.97(5) | 21.05(37) | 13.38(6) | 13.36(4) | 13.43(6) |
| Occ.(T) | 0.909(7) | 0.485(16) | 0.767(8) | 0.764(6) | 0.767(8) |
| $e$(T) | 13.28(9) | 19.21(32) | 15.26(14) | 15.31(10) | 15.27(12) |
| $2{\cdot}e$(M) + $e$(T) | 39.22 | 61.31 | 42.02 | 42.03 | 42.13 |

* $u$ oxygen positional parameter referred to origin at point $\bar{3}m$

$R_{4\sigma}$: residual index for reflections > 4σ; $R_{all}$: residual index for all reflections; $N_{4\sigma}$: reflections > 4σ; $N_{all}$: total number of observed reflections; $U_{ij}$: displacement parameters; $U_{eq}$: equivalent isotropic displacement parameter; Occ.(M), Occ.(T): occupancies in octahedral and tetrahedral sites, respectively (see text); $e$(M), $e$(T): electrons in octahedral and tetrahedral sites, respectively.

Table 2 shows crystallographic data obtained. Residual $R$ factors are calculated using $Fo_{hkl}$ instead of $Fo^2_{hkl}$, for comparison with conventional refinements.

### *Microprobe analysis on XRD crystals*

After data collection, as many analyses as possible were performed on the polished surface of the same single crystal used for the XRD study, in order to obtain the best representative composition of the whole crystal volume. Results are shown in Table 3.

It is noteworthy that, as no chemical constraint from the microprobe data was used during refinements, the agreement between electrons from microprobe and X-ray structure refinement (Tables 2 and 3) was very satisfactory, the difference always being $\leqslant 0.15$.

Concerning TS2, the three crystals selected show that the variability of this sample is still wider than reported in Table 1. However, the differences outlined by microprobe are fully consistent with cell edge variations, that is, a greater $a$ value is related to the relatively higher content of cations of larger size ($Fe^{2+}$ and Cr). The three crystals examined also show a significant difference in the $Fe^{3+}/Fe_{tot.}$ ratio, confirming the variability previously found.

### *Cation distribution from microprobe and XRD data*

Cation distribution between $T$ and $M$ sites was obtained through a minimization program taking into account both X-ray diffraction data and microprobe analyses.

Spinel structure is defined by only two cation-to-oxygen distances, $T$–O and $M$–O, which are related to cell parameter $a$ and to oxygen coordinate $u$ by equations:

$$a = \frac{8}{11\sqrt{3}}\left[5(T-O) + \sqrt{33(M-O)^2 - 8(T-O)^2}\right] \quad (1)$$

$$u = \frac{0.75R - 2 + \sqrt{\frac{33}{16}R - 0.5}}{6(R-1)} \quad (2)$$

where $R = (M\text{–O})^2/(T\text{–O})^2$ (Hafner, 1960).

TABLE 3. Microprobe analysis on XRD single crystals

| | VASA1 | | CR5A1 | | TS2A1 | | TS2E1 | | TS2F1 | |
|---|---|---|---|---|---|---|---|---|---|---|
| | avg. 4 pts. | St.Dev. | avg. 51 pts. | St.Dev. | avg. 5 pts. | St.Dev. | avg. 27 pts. | St.Dev. | avg. 79 pts. | St.Dev. |
| $Al_2O_3$ | 70.08 | 0.25 | 14.50 | 0.36 | 65.33 | 0.18 | 64.81 | 0.28 | 64.61 | 0.71 |
| FeO | 3.93 | 0.15 | 25.83 | 0.30 | 13.43 | 0.38 | 13.08 | 0.22 | 13.62 | 0.27 |
| MgO | 25.39 | 0.25 | 10.07 | 0.14 | 20.58 | 0.28 | 20.91 | 0.15 | 20.16 | 0.28 |
| MnO | 0.13 | 0.04 | 0.22 | 0.13 | 0.11 | 0.05 | 0.10 | 0.04 | 0.10 | 0.03 |
| $SiO_2$ | 0.01 | 0.02 | 0.03 | 0.04 | n.a. | n.a. | 0.02 | 0.01 | 0.03 | 0.01 |
| ZnO | 0.34 | 0.09 | 0.08 | 0.07 | 0.11 | 0.01 | 0.09 | 0.08 | 0.10 | 0.05 |
| $Cr_2O_3$ | 0.01 | 0.02 | 47.64 | 0.69 | 0.33 | 0.01 | 0.23 | 0.09 | 0.50 | 0.03 |
| NiO | 0.04 | 0.03 | 0.10 | 0.05 | n.a. | n.a. | 0.33 | 0.06 | 0.39 | 0.05 |
| $TiO_2$ | 0.01 | 0.01 | 0.59 | 0.05 | 0.04 | 0.01 | 0.02 | 0.02 | 0.05 | 0.08 |
| Total | 99.93 | | 99.06 | | 99.93 | | 99.58 | | 99.56 | |
| Al | 1.996 | 0.004 | 0.556 | 0.012 | 1.935 | 0.002 | 1.924 | 0.007 | 1.927 | 0.012 |
| $Fe^{2+}$ | 0.077 | 0.005 | 0.517 | 0.007 | 0.225 | 0.008 | 0.206 | 0.006 | 0.229 | 0.011 |
| $Fe^{3+}$ | 0.003 | 0.001(*) | 0.187 | 0.009(*) | 0.057 | 0.016(*) | 0.070 | 0.006(*) | 0.059 | 0.006(*) |
| Mg | 0.915 | 0.004 | 0.489 | 0.007 | 0.771 | 0.009 | 0.785 | 0.005 | 0.761 | 0.011 |
| Mn | 0.003 | 0.001 | 0.006 | 0.004 | 0.002 | 0.001 | 0.002 | 0.001 | 0.002 | 0.001 |
| Si | 0.000 | 0.000 | 0.001 | 0.001 | n.a. | n.a. | 0.001 | 0.000 | 0.001 | 0.000 |
| Zn | 0.006 | 0.002 | 0.002 | 0.002 | 0.002 | 0.000 | 0.002 | 0.002 | 0.002 | 0.001 |
| Cr | 0.000 | 0.000 | 1.226 | 0.017 | 0.006 | 0.000 | 0.005 | 0.002 | 0.010 | 0.001 |
| Ni | 0.001 | 0.001 | 0.003 | 0.001 | n.a. | n.a. | 0.007 | 0.001 | 0.008 | 0.001 |
| Ti | 0.000 | 0.000 | 0.015 | 0.001 | 0.001 | 0.000 | 0.001 | 0.000 | 0.001 | 0.001 |
| Total | 3.000 | | 3.000 | | 3.000 | | 3.000 | | 3.000 | |
| $Fe^{3+}/Fe_{tot.}$ | 0.036 | | 0.265 | | 0.202 | | 0.254 | | 0.206 | |
| *e*(chem.)(**) | 39.27 | | 61.41 | | 42.04 | | 42.01 | | 42.28 | |

(*) $Fe^{3+}$ St.Dev. of average, estimated from propagation of errors in other cations.
(**) Total number of electrons calculated from microprobe analyses.

Assuming a linear contribution of each cation in a site to the relative bond distance, $T-O$ and $M-O$ can be expressed as $\sum_i X_i R_{T \text{ or } M,\, i}$ where $X_i$ and $R_{T \text{ or } M,\, i}$ are cation fractions and bond distances respectively. So substitution of these expressions in Equations 1 and 2 gives $a$ and $u$ as functions of $X_i$, once the sizes of the cations involved are known.

The values of $R_{T,\, i}$ and $R_{M,\, i}$ used are reported in Table 4. These values were obtained by the best fit of about 100 lattice parameters of spinels containing the quoted cations (Della Giusta *et al.*, 1996). The following assumptions were made about cation distribution in our spinels: (*a*) Mg, Al, $Fe^{2+}$, $Fe^{3+}$ can occupy both $T$ and $M$ sites; (*b*) Cr occupies only the $M$ site; (*c*) minor cations are assigned only to one site on the basis of their general site preference (i.e. $Si^{4+}$, $Mn^{2+}$ and Zn to the $T$ site; $Ni^{2+}$ and $Ti^{4+}$ to the $M$ site).

Minimization was performed by means of the MINUIT program (Cern Computer Centre, Geneva) which finds the values of parameters corresponding to the minimum of a specific function. The minimized function was:

$$f(X_i) = \sum_{j=1}^{18} \left( \frac{O_j - C_j(X_i)}{\sigma_j} \right)^2 \qquad (3)$$

where $O_j$ is a quantity observed, $C_j(X_i)$ the same quantity calculated by means of parameters $X_i$ and $\sigma_j$ the standard deviation of the observed quantity. The 18 quantities were: $a$, $u$, $e(M)$, $e(T)$, number of cations both per formula unit and in $T$ and $M$ sites (3, 1 and 2 respectively), number of charges for the balance, atomic proportions from microprobe analysis. The $X_i$ parameters chosen were the 14 cation fractions in the two sites.

In the minimization:

(*a*) all parameters were allowed to vary;

(*b*) the starting value was set at 1/2 cation fraction per formula unit in each site, for species possibly in both $T$ and $M$ sites (i.e. disordered), and equal to the cation fraction, for species assigned only to one site;

(*c*) the starting step was set at the starting value or at 2 standard deviations, depending on whether cations were distributed in both sites or only in one;

(*d*) no constraints were imposed for minima and maxima.

Typical runs gave an error sum of squares (*ESS*) of $\sim 1$, each difference between $O_j$ and $C_j(X_i)$ being $\sim 0.2 \cdot \sigma_j$.

For minimization, the average between point analyses was used for VASA1, CR5A1, TS2A1 and TS2F1. Using the average gave unsatisfactory results for TS2E1. This was attributed to a higher $Fe^{3+}/Fe_{tot.}$ ratio (0.25) in comparison with both the Mössbauer measurements and the overall average of the probed sample. This anomalous ratio was probably due to the zoned bands optically evident in the polished surface of the crystal, which may have influenced the average composition in unknown proportions. For this reason, the lower $Fe^{3+}/Fe_{tot.}$ point analysis was tentatively chosen as the best representative of the whole crystal.

Table 5 shows the cation distribution obtained. Not surprisingly, the sum of the residuals was lower in CR5A1 and TS2F1, whose compositions, averaged on many point analyses, are therefore truly representative of the whole crystal volume considered in the XRD study. VASA1 showed highly ordered cation distribution, with almost all divalent iron ($Fe^{3+}$ is virtually absent) in the $T$ site. The number of electrons observed in the $M$ site (12.97) had already indicated little Fe. Mg and Al were also highly ordered, with $\sim 0.12$ Mg atoms in the $M$ site and an equal amount of Al in the $T$ site. CR5A1 also showed good ordering, with $Fe^{2+}$ and $Fe^{3+}$ in $T$ and $M$ sites respectively, and Al only in M site. This suggests that Mg and Al too, if present only in moderate quantities, reside dominantly in T and M sites respectively. A similar distribution of Fe atoms had already been found in chromites from the Bushveld complex (Osborne *et al.*, 1981). TS2 crystals also show good ordering in the distribution, $Fe^{2+}$ being in the $T$ site, $Fe^{3+}$ in the $M$ site, and Al and Mg as in VASA1.

The minimum of function (3) is very sharp in VASA1 and CR5A1, but rather flat in TS2. This is because, in the former samples, there is one more constraint about cations involved in intracrystalline exchange ($Fe^{3+} \cong 0$ in VASA1 and Al confined to the $M$ site in CR5A1). So just one configuration is strongly preferred. Instead, in TS2 all four major cations can occupy both sites and different distributions can give similar values for function (3). In this case, moreover, the set of distances used is crucial:

TABLE 4. Radii $R_T$ and $R_M$ (Å) used in this work

| | Mg | $Fe^{2+}$ | $Fe^{3+}$ | Al | Mn | Si | Zn | Cr | Ni | Ti |
|---|---|---|---|---|---|---|---|---|---|---|
| T site | 1.965 | 1.996 | 1.891 | 1.767 | 2.040 | 1.652 | 1.966 | | | |
| M site | 2.095 | 2.138 | 2.020 | 1.909 | | | | 1.996 | 2.076 | 1.985 |

TABLE 5. Minimization results

| | | Al | $Fe^{2+}$ | $Fe^{3+}$ | Mg | Mn | Si | Zn | Cr | Ni | Ti | *a* | *u* | *e(T)* | *e(M)* | *ESS* |
|---|---|---|---|---|---|---|---|---|---|---|---|---|---|---|---|---|
| VASA1 | obs. | 1.9960 | 0.0765 | 0.0029 | 0.9146 | 0.0026 | 0.0003 | 0.0060 | 0.0002 | 0.0007 | 0.0002 | 8.0930 | 0.26353 | 13.28 | 12.97 | |
| (4 pts.) | calc. | 1.9990 | 0.0743 | 0.0018 | 0.9140 | 0.0026 | 0.0003 | 0.0059 | 0.0002 | 0.0007 | 0.0002 | 8.0931 | 0.26352 | 13.28 | 12.96 | 4.7423 |
| | T | 0.1250 | 0.0730 | 0.0000 | 0.7928 | 0.0026 | 0.0003 | 0.0059 | | | | | | | | |
| | M | 1.8741 | 0.0013 | 0.0018 | 0.1212 | | | | 0.0002 | 0.0007 | 0.0002 | | | | | |
| CR5A1 | obs. | 0.5562 | 0.5165 | 0.1866 | 0.4886 | 0.0059 | 0.0010 | 0.0020 | 1.2260 | 0.0026 | 0.0146 | 8.3017 | 0.26274 | 19.21 | 21.05 | |
| (51 pts.) | calc. | 0.5548 | 0.5167 | 0.1871 | 0.4885 | 0.0061 | 0.0010 | 0.0020 | 1.2268 | 0.0026 | 0.0146 | 8.3017 | 0.26274 | 19.22 | 21.11 | 0.0869 |
| | T | 0.0000 | 0.5031 | 0.0044 | 0.4835 | 0.0061 | 0.0010 | 0.0020 | | | | | | | | |
| | M | 0.5548 | 0.0137 | 0.1827 | 0.0050 | | | | 1.2268 | 0.0026 | 0.0146 | | | | | |
| TS2A1 | obs. | 1.9351 | 0.2251 | 0.0571 | 0.7711 | 0.0024 | 0.0000 | 0.0020 | 0.0065 | 0.0000 | 0.0007 | 8.1104 | 0.26362 | 15.26 | 13.38 | |
| (5 pts.) | calc. | 1.9353 | 0.2237 | 0.0582 | 0.7707 | 0.0024 | 0.0000 | 0.0020 | 0.0065 | 0.0000 | 0.0007 | 8.1105 | 0.26361 | 15.27 | 13.38 | 1.9036 |
| | T | 0.1224 | 0.2205 | 0.0000 | 0.6525 | 0.0024 | 0.0000 | 0.0020 | | | | | | | | |
| | M | 1.8130 | 0.0032 | 0.0582 | 0.1182 | | | | 0.0065 | 0.0000 | 0.0007 | | | | | |
| TS2E1 | obs. | 1.9381 | 0.2217 | 0.0560 | 0.7725 | 0.0020 | 0.0008 | 0.0000 | 0.0031 | 0.0052 | 0.0005 | 8.1081 | 0.26363 | 15.31 | 13.36 | |
| (1 pt.)(*) | calc. | 1.9416 | 0.2206 | 0.0543 | 0.7709 | 0.0019 | 0.0008 | 0.0001 | 0.0031 | 0.0052 | 0.0005 | 8.1084 | 0.26363 | 15.25 | 13.34 | 4.3476 |
| | T | 0.1214 | 0.2206 | 0.0011 | 0.6537 | 0.0019 | 0.0008 | 0.0001 | | | | | | | | |
| | M | 1.8203 | 0.0000 | 0.0532 | 0.1172 | | | | 0.0031 | 0.0052 | 0.0005 | | | | | |
| TS2F1 | obs. | 1.9274 | 0.2289 | 0.0594 | 0.7608 | 0.0021 | 0.0007 | 0.0019 | 0.0100 | 0.0079 | 0.0010 | 8.1122 | 0.26359 | 15.27 | 13.43 | |
| (79 pts.) | calc. | 1.9300 | 0.2256 | 0.0576 | 0.7629 | 0.0021 | 0.0007 | 0.0019 | 0.0099 | 0.0079 | 0.0008 | 8.1122 | 0.26359 | 15.31 | 13.45 | 0.6831 |
| | T | 0.1232 | 0.2233 | 0.0000 | 0.6487 | 0.0021 | 0.0007 | 0.0019 | | | | | | | | |
| | M | 1.8068 | 0.0023 | 0.0576 | 0.1142 | | | | 0.0099 | 0.0079 | 0.0008 | | | | | |

(*) See text.

O'Neill and Navrotsky's set (1983), for example, would predict $Fe^{3+}$ completely in the *T* site. So the calculated $Fe^{3+}$ distribution, if confirmed by Mössbauer spectroscopy, allows us to discriminate between different sets of bond lengths.

## Mössbauer spectroscopy

### *Sample preparation*

Sample VASA did not require particular separation because of the quite large size of its crystals. Sample CR5 at our disposal was already a highly purified concentrate. TS2 spinels were prepared by crushing about 10 g of websterite and retaining two size fractions, one > 125 and < 180, the other > 90 and < 125 μm. Spinels were initially concentrated by passing them twice through a Frantz magnetic separator, and further concentration was achieved by heavy liquid separation. Next, spinels were hand-picked to yield 70 mg of maximum purity concentrates. All three samples were finally crushed and sieved until they passed through a 90-μm aperture sieve. CR5 and TS2 separates were examined by powder X-ray diffraction and no other phases were detected.

### *Experimental*

Materials were suspended in vaseline, wrapped in thin plastic foil, and inserted in a variable-temperature helium cryostat. About 80 mg of the VASA spinel were used in the absorber preparation, 70 for TS2 and 45 for CR5. According to the analytical results, these quantities correspond to 2.5 mg of total iron in the VASA sample and 12 mg in both TS2 and CR5. All spectra were obtained at room temperature (*R.T.*) and at 80.0 K in a conventional constant acceleration spectrometer using a rhodium matrix cobalt-57 source (nominal strength 50 mCi) at *R.T.* The spectrometer was calibrated using natural iron foil at R.T.. Mirror-symmetric spectra were accumulated in a 512 channel analyser, folded, and fitted to pure Lorentzian shapes with the aid of a least-squares fitting program. Peak areas and widths for each quadrupole split doublet were constrained to remain equal, as no preferred orientation is expected for spinels. Computer fits were evaluated by internal consistency across each set of measurements, $\chi^2$, and MISFIT parameters (Ruby, 1973).

The three spinels showed Mössbauer spectra which were rather different from each other and strongly dependent on temperature. They were fitted following a few simple hypotheses. It is well known that, on lowering the temperature, the isomer shift values for both $Fe^{2+}$ and $Fe^{3+}$ increase slightly as a consequence of the second-order Doppler shift. However, while quadrupole splitting of $Fe^{3+}$ compounds (mainly due to the lattice component) remains virtually constant, it increases – sometimes quite strongly – in $Fe^{2+}$ components because of the progressive localization of the '6th' *d* electron on low-lying orbitals. Moreover, a nested doublet configuration, in which the various components have similar δ and different $\Delta E_Q$ values, is always preferred, as it produces fits with reasonable values, in every case falling in the expected ranges.

The VASA spinel gave by far the simplest spectra (Fig. 1), which could easily be fitted to two components due to two different $Fe^{2+}$ species. Spectra at intermediate temperatures were collected to clarify the unexpected temperature dependence of the isomer shift and area ratio.

CR5 spinel produced spectra (Fig. 2) similar to those already reported for lherzolite and Cr-bearing spinels (Wood and Virgo, 1989; Mitra *et al.*, 1991; Osborne *et al.*, 1981). In the *R.T.* spectrum, three well-resolved absorption peaks were evident; moreover, the high-velocity peak clearly derived from the overlap of two smaller ones. However, a fit to only two $Fe^{2+}$ components produced unrealistic results. In any case the microprobe data require the presence of an $Fe^{3+}$ component. At this point, it was straightforward to fit the spectrum to three components, with satisfactory values for the $\chi^2$ and MISFIT parameters. The low-temperature spectrum was somewhat clearer and easier to interpret. As a result of the displacement of the two peaks of each $Fe^{2+}$ doublet toward higher and lower velocities, the high-velocity component of the $Fe^{3+}$ quadrupole split doublet was almost completely resolved. The spectrum was thus satisfactorily fitted to an $Fe^{3+}$ doublet with the same $\Delta E_Q$ as in the *R.T.* spectrum and to two nested $Fe^{2+}$ doublets with δ values slightly increased due to second-order Doppler effects and much larger $\Delta E_Q$.

The TS2 spectra were much more intriguing (Fig. 3). Five different peaks were evident in the 80.0 K spectrum, which also showed a shoulder to the left of the high-velocity peak, while the *R.T.* spectrum showed three broad absorptions. Attempts to obtain good fits with one $Fe^{3+}$ and two $Fe^{2+}$ doublets as in the CR5 case failed, giving too high residuals. As a consequence, a third $Fe^{2+}$ component was added and reasonable parameters were thus obtained for both spectra. Results are reported in Table 6.

### *Results and discussion*

The *R.T.* spectrum of the VASA sample shows two different $Fe^{2+}$ species. Species (1), which dominates the spectral area, is attributable to an $Fe^{2+}$ component in a tetrahedral coordination geometry, in good agreement with the value given by the XRD

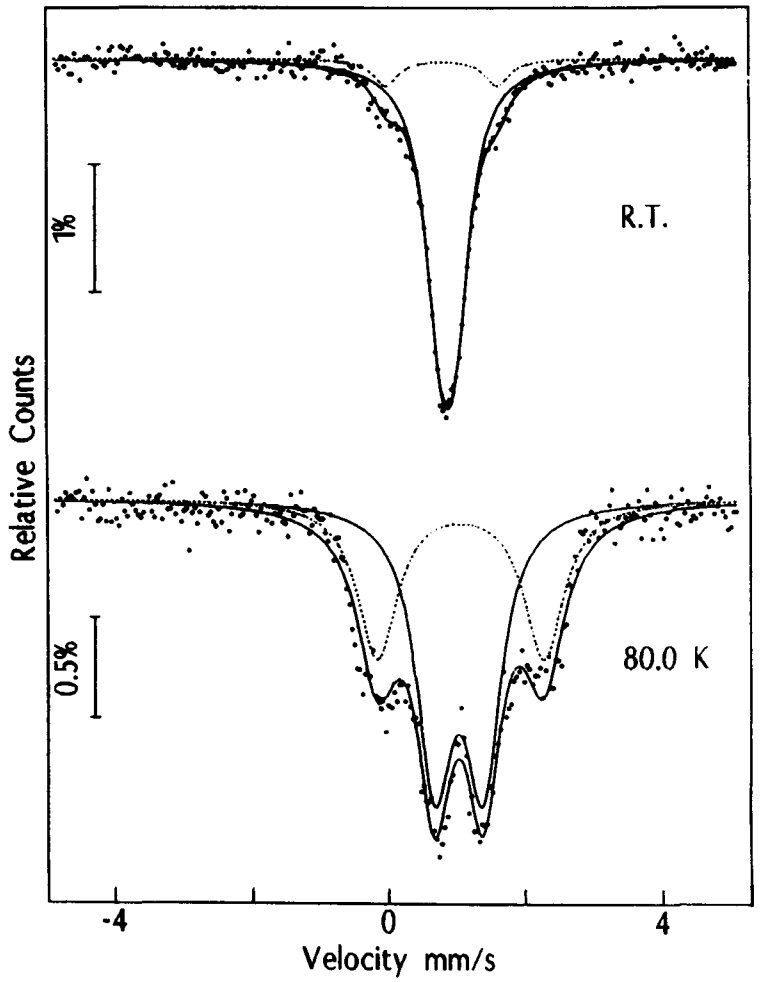


FIG. 1. Mössbauer effect spectra of VASA spinel at *R.T.* and 80.0 K fitted to two tetrahedral $Fe^{2+}$ sites.

data. The very narrow doublet corresponds to an iron centre in practically ideal symmetry, as found in pure $FeCr_2O_4$ (Bancroft *et al.*, 1983; Robbins *et al.*, 1971), in which each oxygen of the tetrahedron is bound to three *M*-site $Cr^{3+}$. Species (2) is found in a much more distorted environment as shown by the larger quadrupole splitting. It also has an isomer shift which is rather low even for a tetrahedral coordination. It was, however, tentatively attributed to a second *T*-site $Fe^{2+}$. These two different tetrahedral sites can be explained with different arrangements of the cations, forming the second coordination sphere. This sphere consists of twelve octahedral sites bonded to the four oxygens. The twelve sites are occupied by Al and Mg (Table 5) in a ratio comparable to the ratio of the areas of the two species (Table 6). On lowering the temperature, the $\Delta E_Q$ values for both sites show the large increase typical for $Fe^{2+}$ derivatives; $\delta$ increases in the same way, although very irregularly, as a consequence of the second-order Doppler shift with a slope which is steeper for species (2) than for species (1). In this way, already at 150.0 K, species (2) has a higher isomer shift than species (1) and in the range characteristic for tetrahedral compounds. The temperature dependence of the relative areas is also somewhat unexpected. The per cent area of species (1) is constant at about 90% down to 220.0 K, and then sharply decreases to 71% at 150.0 K and finally to 60% at 80.0 K. This is a clear indication of great differences in the bonds around the two iron centres: in particular species (2) is constrained in its

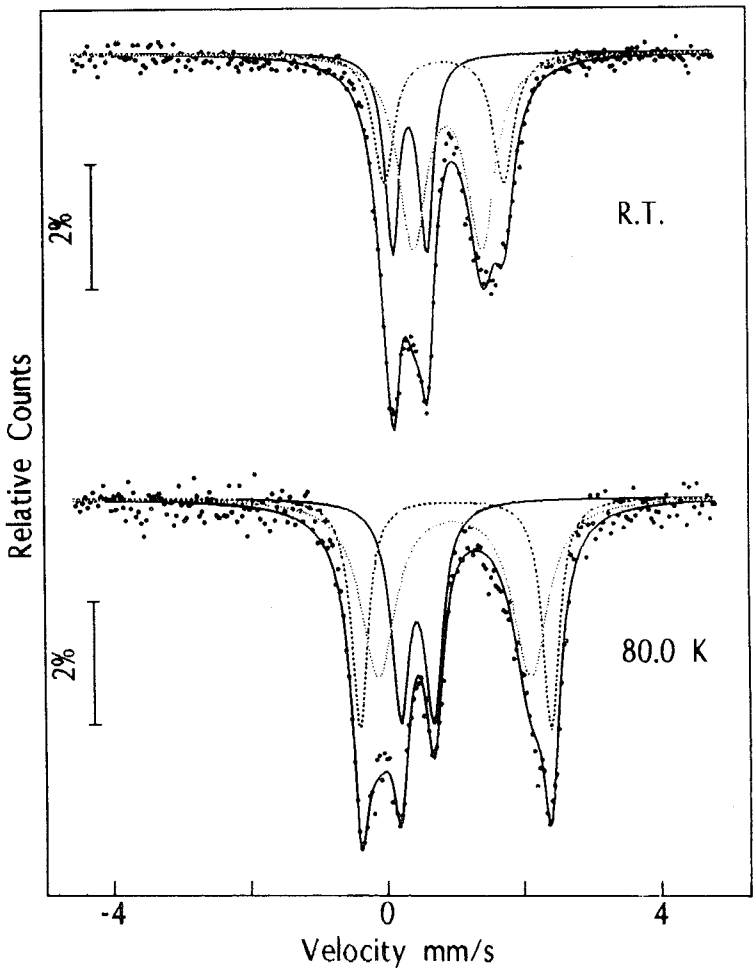


FIG. 2. Mössbauer effect spectra of CR5 spinel at *R.T.* and 80.0 K fitted to one octahedral $Fe^{3+}$ site and two tetrahedral $Fe^{2+}$ sites.

position much less rigidly than that species (1). The bonds around the iron centre probably become longer with increasing temperature: in this way, the strange decrease of both relative area and isomer shift is explained.

The fitted spectra of both TS2 and CR5 include a single $Fe^{3+}$ doublet, with the high-velocity peak partly resolved in the 80.0 K spectra. The isomer shift value of this peak was too high to be considered a singlet, and so a second peak must be hidden inside the low-velocity absorption to give rise to a symmetric doublet; the narrow linewidth of this doublet excludes the presence of other $Fe^{3+}$ species. The $\delta$ value for this doublet was indicative of octahedral coordination, and any attempt to fit this component to tetrahedral values failed. The remaining part of the spectrum is much more complex and ambiguous, and only a tentative interpretation can be given.

The CR5 spectra can reasonably be fitted to two doublets due to $Fe^{2+}$ species with tetrahedral coordination geometry. These two sites, present in an approximate 2:1 ratio, show different distortion, most probably due to the next-nearest neighbour effect. The oxygens of the tetrahedra are probably surrounded by different cations in amounts proportional to their molar fractions. In this way, while the $Fe^{3+}$ octahedral site seems to be surrounded by essentially similar octahedra and tetrahedra, the second coordination sphere of the $Fe^{2+}$ tetrahedral sites is more disordered, as at least a second metal seems to be present.

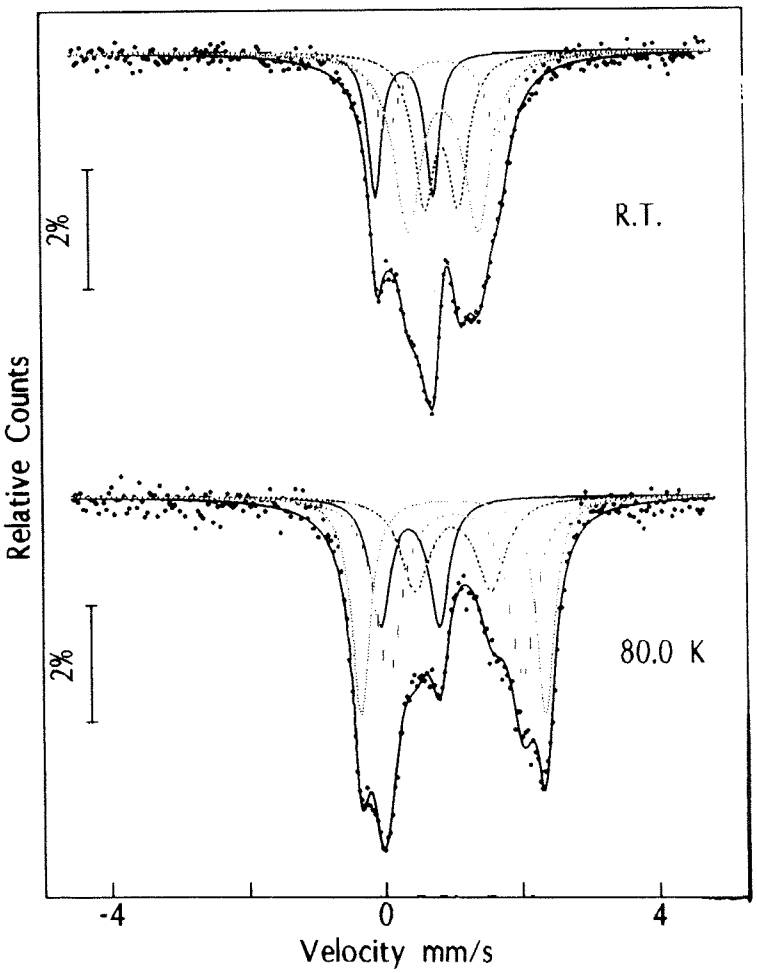


FIG. 3. Mössbauer effect spectra of TS2 spinel at *R.T.* and 80.0 K fitted to one octahedral $Fe^{3+}$ site and three tetrahedral $Fe^{2+}$ sites.

As the TS2 spectra cannot be fitted to only two $Fe^{2+}$ components, a third species is required. This species, absent in the CR5 spectrum, is characterized by very small quadrupole splitting, 0.50 mm/s, and may be attributed to an iron atom in a nearly cubic symmetry that requires the presence of only one type of atoms — Al in this case — in the second coordination sphere. This situation is not possible in the CR5 spinel, because of its different composition. As a consequence, the parameters obtained for the three $Fe^{2+}$ species are less reliable than expected, especially the relative areas. In any case, tetrahedral coordination geometry for all of them is strongly suggested. The environment of the $Fe^{3+}$ site is much more disordered than in the case of CR5, as indicated by the higher $\Delta E_Q$ values. This is consistent with a larger number of possible cation distributions in the second coordination sphere of $Fe^{3+}$, composed of six *T* and six *M* sites. In this case, the *T* site contains three cations in large amounts (see Table 5), while only two are present in CR5.

## Discussion

In order to compare the results obtained by means of the three techniques adopted in this work, it should be recalled that Mössbauer spectroscopy requires large amounts of separated crystals and XRD only a

TABLE 6. Mössbauer effect spectral parameters

| Sample | $T$ K | δ mm/s | $\Delta E_Q$ mm/s | Γ mm/s | $A$ % | Assignment |
|---|---|---|---|---|---|---|
| VASA | *R.T.* | 0.89 | 0.22 | 0.53 | 90 | $Fe^{2+}$(T) (1) |
| | | 0.79 | 1.65 | 0.42 | 10 | $Fe^{2+}$(T) (2) |
| | 220.0 | 0.89 | 0.27 | 0.67 | 89 | $Fe^{2+}$(T) (1) |
| | | 0.86 | 1.93 | 0.40 | 11 | $Fe^{2+}$(T) (2) |
| | 150.0 | 0.92 | 0.46 | 0.61 | 71 | $Fe^{2+}$(T) (1) |
| | | 0.94 | 2.07 | 0.70 | 29 | $Fe^{2+}$(T) (2) |
| | 80.0 | 1.03 | 0.71 | 0.63 | 60 | $Fe^{2+}$(T) (1) |
| | | 1.06 | 2.44 | 0.72 | 40 | $Fe^{2+}$(T) (2) |
| CR5 | *R.T.* | 0.38 | 0.50 | 0.25 | 25 | $Fe^{3+}$(M) |
| | | 0.94 | 1.00 | 0.50 | 50 | $Fe^{2+}$(T) (1) |
| | | 0.90 | 1.76 | 0.36 | 25 | $Fe^{2+}$(T) (2) |
| | 80.0 | 0.45 | 0.49 | 0.32 | 26 | $Fe^{3+}$(M) |
| | | 0.99 | 2.23 | 0.62 | 46 | $Fe^{2+}$(T) (1) |
| | | 1.01 | 2.80 | 0.29 | 28 | $Fe^{2+}$(T) (2) |
| TS2 | *R.T.* | 0.34 | 0.85 | 0.24 | 17 | $Fe^{3+}$(M) |
| | | 0.89 | 0.50 | 0.35 | 25 | $Fe^{2+}$(T) (1) |
| | | 0.91 | 1.03 | 0.47 | 41 | $Fe^{2+}$(T) (2) |
| | | 0.92 | 1.64 | 0.42 | 17 | $Fe^{2+}$(T) (3) |
| | 80.0 | 0.37 | 0.87 | 0.35 | 18 | $Fe^{3+}$(M) |
| | | 1.01 | 1.11 | 0.52 | 19 | $Fe^{2+}$(T) (1) |
| | | 1.04 | 1.96 | 0.47 | 34 | $Fe^{2+}$(T) (2) |
| | | 1.00 | 2.70 | 0.32 | 29 | $Fe^{2+}$(T) (3) |

single fragment, while microprobe analyses can be performed on many crystals and many spots of a single crystal. In the case of significant sample heterogeneity, as in ours, it is essential to exert great caution in ascertaining which analysis can best represent the sample.

The quantities to be compared are: (*a*) the $Fe^{3+}/Fe_{tot.}$ ratio, observed in Mössbauer spectra and calculated from microprobe analyses averaged on many crystals; (*b*) the $Fe^{2+}$, $Fe^{3+}$ site populations measured in Mössbauer and calculated from XRD plus microprobe data on a single crystal.

Comparison (*a*) can be done by looking at Tables 1 (bottom rows) and 6. If the ratios are considered together with their errors, the agreement in CR5 sample is very close; in VASA and TS2 it is quite satisfactory, bearing the previous observations in mind. $Fe^{3+}$ calculated by stoichiometry from microprobe analyses seems to be slightly overestimated. This, at least in part in sample TS2, is due to the presence of a few hematite lamellae (< 1 μm thick) in some fragments. This presence is not detectable either by XRD or Mössbauer, but is apparent under the microscope and is responsible for contamination of the spinel sample, leading to an excess of iron atoms.

Such results therefore suggest that, unlike Wood and Virgo (1989) and Dyar *et al.* (1989), sufficient accuracy can also be achieved by means of microprobe, provided that analyses are performed on adequate populations and carefully prepared grain mounts after suitable calibration.

Comparison (*b*) is summarized in Table 7, in which data from *R.T.* Mössbauer spectra are reported because percent areas of $Fe^{3+}$ and total $Fe^{2+}$ are not significantly affected by temperature. Mössbauer results were corrected taking into account the ratio between the recoil-free fractions of $T$ and $M$ sites. Various values for this ratio have been published with the aim of taking into account the different bonds in the two cases. All of them are slightly lower than 1 at *R.T.* and do not affect the results significantly. The value used here was 0.94 (Sawatzky *et al.*, 1969). The agreement between experimental evidence and calculated distributions for $Fe^{2+}$, $Fe^{3+}$ shows the substantial correctness of the model used in the minimization process, particularly for the set of bond distances employed, and consequently of the overall site populations. Moreover, both Mössbauer and XRD indicate strong ordering of $Fe^{2+}$ in the $T$ site and $Fe^{3+}$ in the $M$ site in these samples. It is noteworthy that there is

TABLE 7. Comparison of Fe percent distribution between Mössbauer spectroscopy, taking into account recoil-free fraction differences of *T* and *M* sites (see text), at *R.T.* (observed) and XRD plus microprobe results (calculated), relative to $Fe_{tot.}$

| | | $Fe^{2+}$(T) | $Fe^{2+}$(M) | $Fe^{3+}$(T) | $Fe^{3+}$(M) | $Fe^{3+}$(T+M) |
|---|---|---|---|---|---|---|
| VASA | obs. | 100 | 0 | 0 | 0 | 0 |
| VASA1 | calc. | 95.9 | 1.7 | 0.0 | 2.4 | 2.4 |
| CR5 | obs. | 73 | 0 | 0 | 27 | 27 |
| CR5A1 | calc. | 71.5 | 1.9 | 0.6 | 26.0 | 26.6 |
| TS2 | obs. | 82 | 0 | 0 | 18 | 18 |
| TS2A1 | calc. | 78.2 | 1.1 | 0.0 | 20.6 | 20.6 |
| TS2E1 | calc. | 80.2 | 0.0 | 0.4 | 19.4 | 19.8 |
| TS2F1 | calc. | 78.9 | 0.8 | 0.0 | 20.3 | 20.3 |

better agreement here between $Fe^{3+}/Fe_{tot.}$ ratios than in comparison (*a*). In the case of TS2, this is probably due to the fewer inclusions or hematite lamellae in the crystals chosen for the XRD study than in the bulk analyses.

Mössbauer spectroscopy is extremely sensitive to small variations in electron density at the iron nucleus, due to different electronic and structural environments. It does not average the various situations, as in the case of XRD, but it does sum the various contributions that can be extracted from the overall spectrum. In this way it is possible, for these spinels at least, to detect the presence of different coordination tetrahedra around the $Fe^{2+}$ centres, attributable to the next-nearest neighbour effect. The existence of various iron sites may well be the consequence of the conditions in which these materials formed. Thus, relatively slow cooling and the presence of a large variety of cations with similar solubility should favour the formation of numerous coordination geometries, clearly detected in Mössbauer spectra.

## Acknowledgements

The authors have greatly benefited by advice and comments of Piergiorgio Jobstraibizer, Pietro Frizzo, and Enzo M. Piccirillo during the preparation of this work. Thanks are due to Gabriella Demarchi and Piero Comin-Chiaramonti for providing TS2 sample. Bengt Lindqvist (Swedish Museum of Natural History) kindly informed us of place of origin of VASA sample. S. C. thanks in particular her husband for great help. Raoul Carampin kindly assisted in the microanalysis. The authors also gratefully acknowledge the financial support of the Italian Consiglio Nazionale delle Ricerche (CNR Centro di Studio per la Geodinamica Alpina, Padova) and the Ministero dell'Università e della Ricerca Scientifica e Tecnologica.

## References

Bancroft, G.M., Osborne, M.D. and Fleet, M.E. (1983) Next-nearest neighbour effects in the Mössbauer spectra of Cr-spinels: an application of partial quadrupole splittings. *Solid State Comm.*, **47**, 623–5.

Blessing, R.H., Coppens, P. and Becker, P. (1972) Computer analysis of step-scanned X-ray data. *J. Appl. Crystallogr.*, **7**, 488–92.

Comin-Chiaramonti, P., Demarchi, G., Siena, F. and Sinigoi, S. (1982) Relazioni tra fusione e deformazione nella peridotite di Balmuccia (Ivrea-Verbano). *Rend. Soc. Ital. Mineral. Petrol.*, **38**, 685–700.

Della Giusta, A., Carbonin, S. and Ottonello, G. (1996) Temperature-dependent disorder in natural Mg-Al-$Fe^{2+}$-$Fe^{3+}$ spinel. *Mineral. Mag.*, in press.

Dyar, M.D., McGuire, A.V. and Ziegler, R.D. (1989) Redox equilibria and crystal chemistry of coexisting minerals from spinel lherzolite mantle xenoliths. *Amer. Mineral.*, **74**, 969–80.

Hafner, S. (1960) Metalloxyde mit Spinellstruktur. *Schweiz. Mineral. Petrol. Mitt.*, **40**, 208–40.

Mason, T.O. (1987) Cation intersite distributions in iron-bearing minerals via electrical conductivity/Seebeck effect. *Phys. Chem. Minerals*, **14**, 156–62.

Millard, R.L., Peterson, R.C. and Hunter, B.K. (1992) Temperature dependence of cation disorder in $MgAl_2O_4$ spinel using $^{27}Al$ and $^{17}O$ magic-angle spinning NMR. *Amer. Mineral.*, **77**, 44–52.

Mitra, S., Pal, T. and Pal, T. (1991) Petrogenetic implication of the Mössbauer hyperfine parameters

of $Fe^{3+}$-chromites from Sukinda (India). *Mineral. Mag.*, **55**, 535–42.

Nell, J., Wood, B.J. and Mason, T.O. (1989) High temperature cation distributions in $Fe_3O_4$–$MgAl_2O_4$–$MgFe_2O_4$–$FeAl_2O_4$ spinels from thermopower and conductivity measurements. *Amer. Mineral.*, **74**, 339–51.

North, A.C.T., Phillips, D.C. and Scott-Mattews, F. (1968) A semi-empirical method of absorption correction, *Acta Crystallogr.*, **A24**, 351–2.

O'Neill, H.St.C. and Navrotsky, A. (1983) Simple spinels: crystallographic parameters, cation radii, lattice energies, and cation distribution. *Amer. Mineral.*, **68**, 181–94.

O'Neill, H.St.C. and Navrotsky, A. (1984) Cation distributions and thermodynamic properties of binary spinel solid solutions. *Amer. Mineral.*, **69**, 733–53.

O'Neill, H.St.C., Dollase, W.A. and Ross, C.R.II (1991) Temperature dependence of the cation distribution in Nickel Aluminate ($NiAl_2O_4$) spinel: a powder XRD study. *Phys. Chem. Minerals*, **18**, 302–19.

O'Neill, H.St.C., Annersten, H. and Virgo, D. (1992) The temperature dependence of the cation distribution in magnesioferrite ($MgFe_2O_4$) from powder XRD structural refinements and Mössbauer spectroscopy. *Amer. Mineral.*, **77**, 725–40.

Osborne, M.D., Fleet, M.E. and Bancroft, G.M. (1981) $Fe^{2+}$ -$Fe^{3+}$ ordering in chromite and Cr-bearing spinels. *Contrib. Mineral. Petrol.*, **77**, 251–5.

Ottonello, G. (1986) Energetics of multiple oxides with spinel structure. *Phys. Chem. Minerals*, **13**, 79–90.

Peterson, R.C., Lager, G.A. and Hitterman, R.L. (1991) A time-of-flight neutron powder diffraction study of $MgAl_2O_4$ at temperatures up to 1273 K. *Amer. Mineral.*, **76**, 1455–8.

Pizzolon, M. (1991) *Cristallochimica e Modellizzazione di Spinelli di Mg-Al-Fe-Cr.* Thesis, University of Padova, Padua, Italy.

Robbins, M., Wertheim, G.K., Sherwood, R.C. and Buchanan, D.N.E. (1971) Magnetic properties and site distribution in the system $FeCr_2O_4$ - $Fe_3O_4$. *J. Phys. Chem. Solids*, **32**, 717–29.

Roelofsen, J.N., Peterson, R.C. and Raudsepp, M. (1992) Structural variation in nickel aluminate spinel ($NiAl_2O_4$). *Amer. Mineral.*, **77**, 522–8.

Ruby, S.L. (1973) Why MISFIT when you already have $\chi^2$? *Mössbauer Effect Methodology*, **8**, 263–76.

Sawatzky, G.A., van der Wonde, F. and Morrish, A.H. (1969) Recoiless-fraction ratios for $^{57}Fe$ in octahedral and tetrahedral sites of a spinel and a garnet. *Phys. Rev.*, **183**, 383–6.

Sheldrick, G.M. (1993) SHELX-93. Program for crystal structure refinement, University of Göttingen, Germany.

Skogby, H., Annersten, H., Domeneghetti, M.C., Molin, G.M. and Tazzoli, V. (1992) Iron distribution in orthopyroxene: a comparison of Mössbauer spectroscopy and X-ray refinement results. *Eur. J. Mineral.*, **4**, 441–52.

Toffanin, N. (1989) *Studio Cristallochimico di Cromiti in Complessi Stratiformi ed Ofiolitici.* Thesis, University of Padova, Padua, Italy.

Waerenborgh, J.C., Figueiredo, M.O., Cabral, J.M.P. and Pereira, I.C.J. (1994) Powder XRD structure refinements and $^{57}Fe$ Mössbauer effect study of synthetic $Zn_{1-x}Fe_xAl_2O_4$ ($0 < x \leqslant 1$) spinels annealed at different temperatures. *Phys. Chem. Minerals*, **21**, 460–8.

Wood, B.J. and Virgo, D. (1989) Upper mantle oxidation state: ferric iron contents of lherzolite spinels by $^{57}Fe$ Mössbauer spectroscopy and resultant oxygen fugacities. *Geochim. Cosmochim. Acta* , **53**, 1277–91.

[*Manuscript received 4 January 1995: revised 18 April 1995*]